Progress In Electromagnetics Research B, Vol. 34, 145–171, 2011

NUMERICAL MODELLING FOR ULTRA WIDEBAND RADAR BREAST CANCER DETECTION AND CLASSIFICATION

R. C. Conceição[1, 2], M. O'Halloran[1, 2, *], M. Glavin[1, 2], and E. Jones[1, 2]

[1]Electrical and Electronic Engineering, College of Engineering and Informatics, National University of Ireland Galway, Ireland

[2]Bioelectronics Research Cluster, NCBES, National University of Ireland Galway, Ireland

Abstract—Microwave Imaging is one of the most promising emerging imaging technologies for breast cancer detection, and exploits the dielectric contrast between normal and malignant breast tissue at microwave frequencies. The development of many UWB Radar imaging approaches requires the use of accurate numerical models for the propagation and scattering of microwave signals within the breast. The Finite-Difference Time-Domain (FDTD) method is the most commonly used numerical modelling technique used to model the propagation of Electromagnetic (EM) waves in biological tissue. However, it is critical that an FDTD model accurately represents the dielectric properties of the constituent tissues, including tumour tissues, and the highly correlated distribution of these tissues within the breast. This paper presents a comprehensive review of the latest findings regarding dielectric properties of normal and cancerous breast tissue, and the heterogeneity of normal breast tissue. Furthermore, existing FDTD models of the breast described in the literature are examined.

1. INTRODUCTION

Breast cancer is one of the most common cancers to affect women. In the United States alone, it accounts for 31% of new cancer cases, and is second only to lung cancer as the leading cause of deaths in American women [1]. More than 184,000 new cases of breast

Received 27 July 2011, Accepted 29 August 2011, Scheduled 11 September 2011

* Corresponding author: Martin O'Halloran (martin.ohalloran@gmail.com).

cancer are diagnosed each year resulting in approximately 41,000 deaths [1]. At the same time, breast cancer mortality is on the decline in industrialised countries such as the United States, Canada, Germany, Austria and the United Kingdom [2]. This decline can be partly attributed to increased breast cancer screening, and the early detection and treatment of the disease. Consequently, early detection and intervention is one of the most significant factors in improving the survival rates and quality of life experienced by breast cancer sufferers [2], since this is the time when treatment is most effective.

The current standard screening method for detecting non-palpable early stage breast cancer is X-ray mammography. Despite the fact that X-ray mammography provides high resolution images using relatively low radiation doses, its limitations are well documented [2]. The search for new imaging techniques is motivated by the need for increased specificity and sensitivity, especially in the case of radiographically dense tissue. Issues also exist with the alternative imaging technologies: MRI and Ultrasound. Despite the fact that recent research has shown that MRI has a negative predictive value of 99% [3], the cost and issues with the sensitivity and specificity of these alternative imaging modalities, particularly ultrasound, preclude their widespread use [4, 5].

One of the most promising emerging breast imaging modalities is microwave imaging. Three alternative active microwave imaging techniques are under development: Hybrid Microwave-Induced Acoustic imaging, Microwave Tomography and Ultra Wideband (UWB) Radar imaging. The hybrid imaging method involves heating any tumours present in the breast using microwave signals, and using ultrasound transducers to record the resultant pressure waves due to the heat-induced expansion of the tumour tissue. Based on these recorded waves, the presence and location of the tumours can be identified [6]. Microwave Tomography involves reconstructing the complete dielectric profile of the breast using a forward and inverse scattering model [7–11]. Finally, UWB Radar imaging, as proposed by [12], uses reflected UWB signals to determine the location of microwave scatterers within the breast.

The research and development of these imaging approaches requires accurate FDTD breast phantoms to model the propagation and scattering of microwave signals within the breast, and generates representative backscattered signals. The FDTD method has become the *de facto* numerical method for modelling the propagation of electromagnetic signals in biological tissue. FDTD breast models must incorporate the geometrical properties of the breast, the natural heterogeneity of the breast structure and the dispersive properties of

breast tissue. Similarly, tumour models must incorporate the shape, surface texture and growth pattern of benign and malignant tumours. This paper presents a comprehensive survey of recent research on the dielectric properties of normal breast and tumour tissue, and discusses the numerical modelling of the breast using these properties. The structure of the paper is as follows: Section 2 examines the anatomy and physiology of the breast; Section 3 describes breast cancer and tumour formation; Section 4 describes the dielectric properties, tumour and breast modelling; finally, Section 5 discusses the conclusions and suggestions for future work.

2. ANATOMY AND PHYSIOLOGY OF THE BREAST

The breast is mainly composed of three types of tissue: breast fat (or adipose tissue), glandular tissue and connective tissue (fibrous strands called Cooper's ligaments). The proportions of these main types of tissue may vary from person to person [13–15] and the amount of water, fat and fibroglandular tissue may also vary due to normal hormonal changes in different stages of menstruation, pregnancy, lactation or menopause [13, 16]. For the purpose of bioelectrical studies, the anatomy of the breast can be simplified and presented as follows:

- Below the skin there is an adipose tissue layer which consists of vesicular cells filled with fat which are collected into lobules and then separated by Cooper's ligaments.
- The innermost tissue of the breast consists of mammary glands (lobules that produce milk). Each breast has about 15 to 20 sections termed lobes with many smaller sections of mammary glands, which are arranged in a circular fashion. Each Section is terminated by thin tubes, called lactiferous ducts, which connect to a reservoir (also called ampulla) and ultimately connect to the nipple. These lobes and ducts are also surrounded by Cooper's ligaments.
- Cooper's ligaments also have the function of maintaining the inner structure of the breast and supporting the tissue attached to the chest wall. The breast is separated from the pectoralis major muscle by the retromammary fat [17].

The anatomy of a healthy breast in both frontal and sagittal views is shown in Figure 1. It should be noted that although lymph nodes are not constituents of the breast *per se*, they are represented in this figure as breast cancer can be diagnosed through detection of metastasised tumour cells particularly in the axillary lymph nodes, where approximately 50% of breast cancer occur [18, 19].

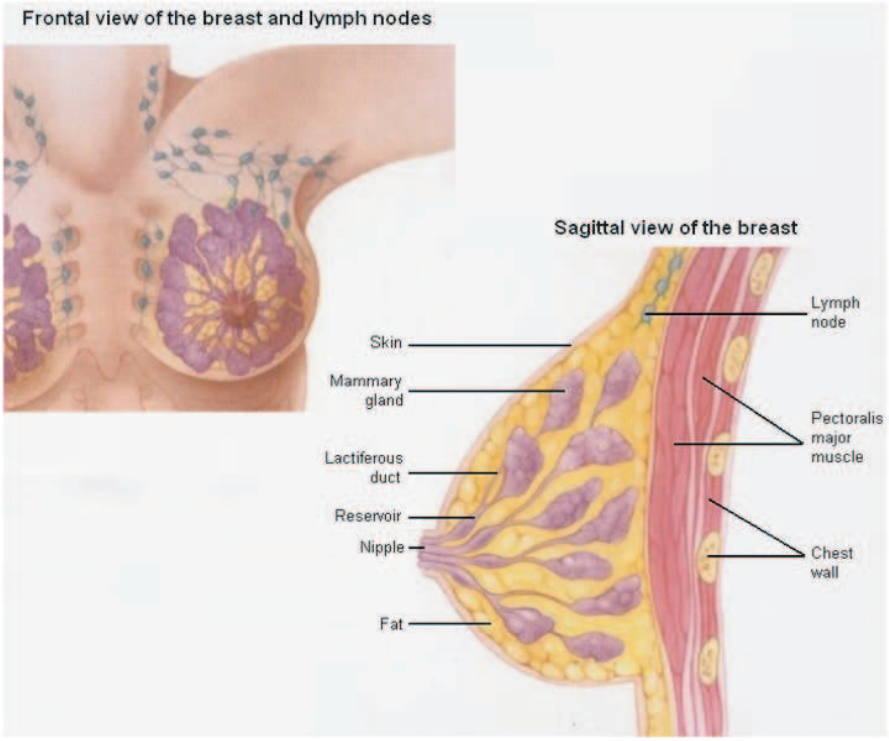

Figure 1. General anatomy of the breast in frontal and sagittal views (adapted from [20]).

3. DEVELOPMENT AND GROWTH PATTERNS OF BREAST CANCER

3.1. Breast Cancer

Breast cancer is more likely to develop in older women [21]. This is due to the fact that cells have to undergo multiple genetic alterations before a cell becomes malignant [22]. There is also a higher incidence of breast cancer if previous family generations suffered from the disease (family history) and also if the patient previously developed breast or any other type of cancer [21].

The two most common types of cancer are: invasive and *in situ* (or non-invasive). Invasive cancers are those in which there is dissemination of cancer cells outside the basement membrane of the ducts and lobules into the surrounding adjacent normal tissue. *In situ* cancers are those in which cancer cells remain within the basement

membrane of the lobules and the draining lactiferous ducts [23].

Some of the most frequently-occurring breast cancers are as follows [23]:

- Invasive Ductal Carcinoma (IDC) is the most common type of breast cancer (70 to 80% of breast cancer cases), and occurs in the cells that line the ducts of the breasts.
- Invasive Lobular Carcinoma (ILC) represents about 10% of breast cancer cases and occurs in the cells that line the lobules of the breast.
- The Ductal Carcinoma *In Situ* (DCIS) is a type of cancer in which cancerous cells are inside some of the ducts, but have not spread to other regions of the breast or body.
- The Lobular Carcinoma *In Situ* (LCIS) is not a type of cancer *per se*, but in presence of this disease there are high chances of developing cancer. LCIS is characterised by changes in the cells within the breast lobes.

These types of breast tumours are shown in a simplified sagittal view of the breast in Figure 2.

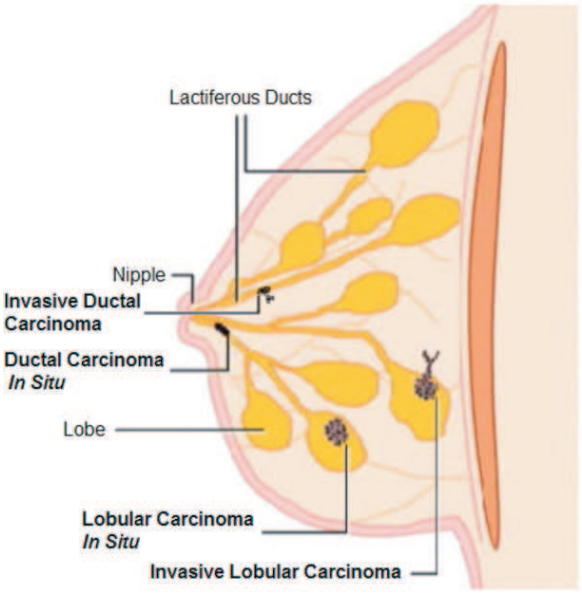

Figure 2. Simplified sagittal view of the breast with representative examples of two of the most common types of breast tumour: in situ and invasive. Image adapted from [20].

3.2. Tumour Formation

Tumours are defined by a growth of undifferentiated (or unspecialised) cells which form a lump. Usually the immune system is capable of destroying the undifferentiated cells which can lead to the formation of a tumour through a process called apoptosis — cell self-destruction. However, if too many mutations occur in cells at the same time, the immune system may not be able to respond appropriately, and masses of tumour cells will be formed [24].

The way proliferation of tumour cells occurs, i.e., the tumour growth, may indicate whether a tumour is benign or malignant. For benign tumours, the growth is controlled and will only be dangerous if nearby organs are pushed and compressed or if tumours either grow inside the skull or release unwanted hormones. Conversely, for malignant tumours, i.e., cancer, the growth is uncontrolled due to a high rate of replication and usually spreads to other parts of the body by metastases and destroys surrounding healthy tissues [24].

The tumour cell suffers several changes in terms of cell surface, the state of water, viscosity, pH, growth regulation, the loss of contact inhibition, the cytoskeleton, temperature, membrane transport, and several other factors [13, 25]. The grade of malignancy of the tumour can be determined by pathologically analysing how premature the cells are within the tumour. The less mature the tumour cells, the older and more widespread the malignant tumour is likely to be, and therefore the lower the chances of successful treatment. The different grades of development at which cells can be found is referred to as differentiation [24].

The cytoskeleton of tumour cells becomes disorganised due to the decrease and disorganisation of microfilaments and microtubules [25], causing the original shape of the cell to be lost (becoming more round) and the process of mitosis (cell replication) to become chaotic leading to both an uncontrolled growth of tissues and the loss of genetic information. Because the surface of the cells changes, the membrane permeability is altered and the regular osmosis process is also affected, causing the tumour tissues to retain more fluid than normal cells. Cancer cells retain more fluid in the form of bound water, which ultimately affects the dielectric properties of the tissue.

Additionally, cancer cells are not contact-inhibited, which means that huge masses of cancer cells grow over each other forming multiple layers, and are able to coexist in high concentrations. Furthermore, due to the large growth of cells in tumours, particularly in malignant tumours, networks of capillaries are created in order to nourish the newly formed cells [26]. In [27], it is noted that neoangiogenesis (growth of new blood vessels) is induced by tumours with a dimension of at

least 3 mm. As the size of tumours becomes larger, these networks of capillaries may be developed into tiny veins and even arteries that will connect to major blood supply vessels [26], therefore the study of the level of vascularisation near a tumour is of importance to the characterisation of the grade of malignancy of a tumour.

The increase of water within cancerous tissue is responsible for the high scattering in microwave imaging. The increase of sodium and water, particularly in bound water, within the tumour cell induces greater values of conductivity and relative permittivity in tumour tissues [14, 28, 29]. Another feature that may help detect the presence of malignant tumours is the existence of calcifications. However these are only formed when severe necrosis has occurred, i.e., disorderly apoptosis, resulting in groups of dead cells which are not naturally absorbed by the organism [14].

Finally, other characteristics inherent to benign and malignant tumours have proven to be useful in terms of classification for different imaging modalities. Such characteristics are based on size [17, 26, 27, 30, 31], shape [17, 30, 31], margins [30, 31], surface texture [30, 31], depth [27], localisation [27, 31] and packing density [27, 31]. Features of a tumour that may be of particular benefit for classification in the context of microwave imaging are the shape and texture of the tumour surface. Malignant tumours usually present the following characteristics:

- Irregular, ill-defined and asymmetric shapes;
- Blurred boundaries (lack of sharpness);
- Rough and complex surfaces with spicules or microlobules;
- Non-uniform permittivity variations;
- Distortion in the architecture of the breast;
- Irregular increase of tissue density (due to masses and calcifications).

Conversely, benign tumours tend to have the following characteristics:

- Spherical, oval or at least present well-circumscribed contours;
- Compact;
- Smooth surfaces [26, 31–34].

Accurate modelling of these characteristics is important for the development of microwave imaging systems.

4. MODELLING

In this section, the dielectric properties of the breast, and methods to model the dielectric and anatomical properties of the breast and tumours are discussed.

4.1. Dielectric Properties

The dielectric properties (conductivity and relative permittivity) determine the transmission, reflection and attenuation of microwave signals as they propagate through the breast, permitting the differentiation between different types of tissue within the breast at microwave frequencies. Several historical studies have been completed examining the *in vivo* and *ex vivo* dielectric properties of normal and malignant breast tissues. An extensive review of these studies was previously completed by the authors [35]; in this paper more recent studies are discussed and the effect of their findings on previous literature is considered.

In 2000, Meaney et al. [9] performed the first *in vivo* dielectric study using a prototype microwave imaging system. A 16 element monopole antenna array was used in a tomographic microwave imaging system operating in the 300 to 1000 MHz frequency range. Results at 900 MHz are shown in Table 1 and it can be observed that the average relative permittivity value is significantly higher, approximately between 31 and 36, than that published in an earlier study by Joines et al. [36].

More recently, Lazebnik et al. [15, 37] completed one of the most comprehensive studies to date on dielectric properties of the breast. The first study [15] focused on the dielectric properties of normal

Table 1. Average dielectric properties of female breast tissue at 900 MHz measured in vivo using an active microwave imaging system developed by Meaney et al. [9].

Patient	Age	Average relative permittivity (%)	Average conductivity (Sm^{-1})
1	6	17.22 ± 11.21	0.5892 ± 0.3547
2	57	31.14 ± 4.35	0.6902 ± 0.3650
3	52	36.44 ± 6.24	0.6869 ± 0.3156
4	49	35.43 ± 3.93	0.5943 ± 0.3841
5	48	30.85 ± 7.22	0.6350 ± 0.3550

breast tissue, and the second study [37] focused on the dielectric contrast between normal, benign and malignant breast tissues. In both studies, the data were mapped to Cole-Cole models. Hoping to improve on many of the apparent weaknesses of previous studies, such as small patient sample sizes and gaps in the frequency bands examined, Lazebnik histopathologically analysed a large sample of freshly excised breast tissue from surgical patients and divided normal tissue samples into 3 groups, distinguishing each by the percentage of adipose, glandular and fibroconnective tissue contained in the sample before obtaining the values for the dielectric properties. The three groups were defined as follows:

- Group 1 contains samples with 0–30% adipose tissue;
- Group 2 contains samples with 31–84% adipose tissue;
- Group 3 contains samples with 85–100% adipose tissue.

The results of the first study are shown in Figure 3, which summarises the permittivity and conductivity as a function of frequency, for normal breast tissue. By comparing these results to previous dielectric studies, Lazebnik's main conclusions were as follows:

- The dielectric properties found for normal tissue in the samples of Group 3 (the highest adipose content) were lower than any previous studies.
- The dielectric properties found for normal tissue in the samples of Group 1 (the highest fibroglandular content) were higher than any previous studies.
- The dielectric data spanned a much greater range of values than those reported in previous studies, with the exception of Campbell and Land's study [38].

Overall, Lazebnik attributed these differences to the large heterogeneity in normal breast tissue, as previously noted in [38], and acknowledged the relationship between fibroglandular content and average dielectric properties.

In the second study, Lazebnik et al. [37] examined the differences between normal, benign and malignant tumours across a frequency range of 0.5 to 20 GHz. Normal breast tissue included adipose, glandular and fibroconnective tissues; benign tumour tissue included fibroadenoma and cysts; and, finally, malignant tumour included ductal and lobular carcinomas (IDC, DCIS, ILC and LCIS). The results are shown in Figure 4.

From the study in [37], Lazebnik et al. first observed that measured dielectric values for malignant tissue were in general agreement with the studies by Chaudhary et al. [39], Surowiec et

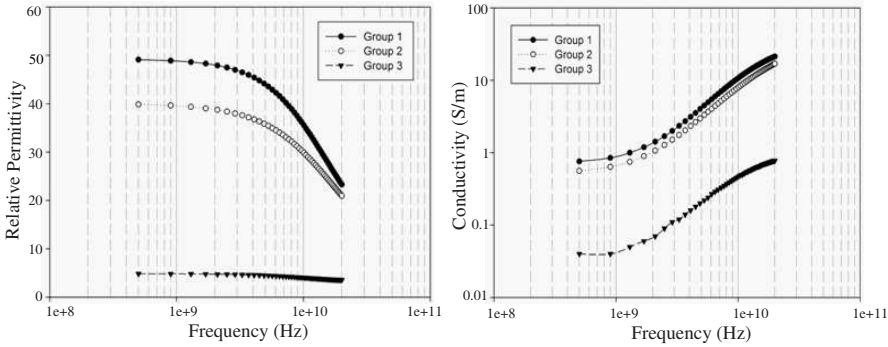

Figure 3. The relative permittivity (a) and conductivity (b) of normal breast tissue as measured by Lazebnik et al. [15] over the frequency band 0.5 to 20 GHz. Group 1 represents 0–30% adipose tissue, group 2 represents 31–84% adipose and group 3 represents 85–100% adipose tissue.

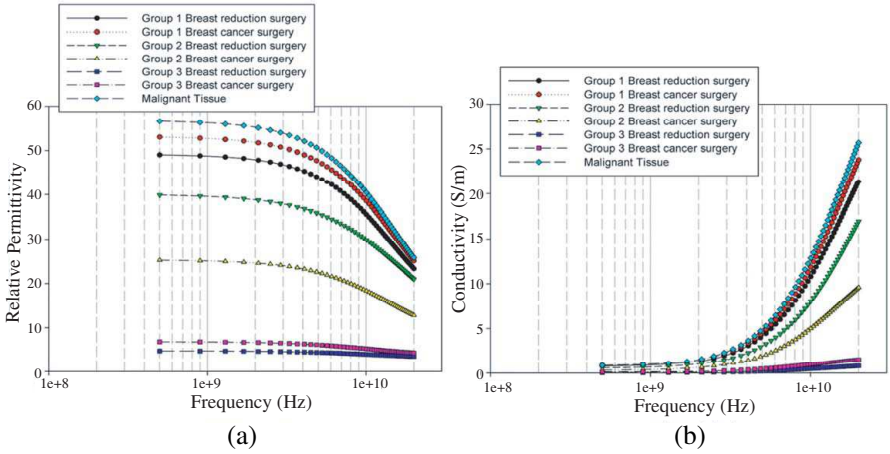

Figure 4. The median relative permittivity (a) and conductivity (b) Cole-Cole curves for groups 1, 2 and 3 for normal tissue obtained from reduction surgeries and cancer surgeries. The median relative permittivity curve of the dielectric properties of samples that contained at least 30% malignant tissue content is also shown for comparison. All results correspond to the 50th percentile [37].

al. [40] and Joines et al. [36]. Furthermore, Lazebnik et al. justified the differences between the curves for group 2 observed in Figure 4 as an experimental error due to the comparatively small sample size used in the cancer surgery study compared to the breast reduction surgery study, which varied from 16 to 84 samples. Also, it was acknowledged in [37] that the dielectric properties for normal tissues obtained through breast cancer surgery were lower than those obtained in breast reduction surgery and it was suggested that this was due to the fact that tumours usually develop in glandular tissue and consequently the non-affected tissues removed (from a region distinct from the tumour) had comparatively higher adipose content.

Finally, by adjusting for the content of adipose tissue within the samples Lazebnik et al. found that there only existed a 10% difference between the conductivity of normal tissue and malignant tissue, and an approximate 8% difference in relative permittivity at 5 GHz. However, by adjusting for the content of both adipose and fibroconnective tissues within the samples, they found no statistical difference between normal fibroglandular and malignant tumour tissues in the breast. The high dielectric properties of benign/fibroglandular tissue overlap those of malignant tissue within the breast, and consequently could materialise as 'false positive' results in UWB images, creating a much more difficult imaging scenario than previously believed.

Overall, the studies in [15, 37] greatly added to the knowledge of breast tissue dielectric properties by significantly increasing the population size, by having separate analysis depending on the proportion of different types of tissues within the breast, and by characterising the tissues across a wide frequency band between 0.5 and 20 GHz. In [15, 37], a very detailed database of dielectric properties based on Cole-Cole parameters was established for each tissue type, which is crucial to accurately develop a numerical breast phantom, described later in this paper.

In addition, in 2009, Halter et al. [41] presented the initial results from a clinical study with a smaller number of patients in which estimates of the dielectric properties of malignant breast tissue were obtained in three different scenarios. The dielectric properties were taken in the following scenarios: (i) by estimation means of Electrical Impedance Tomography imaging, (ii) by direct measurement *in vivo* breast cancer using both Electrical Impedance Spectroscopy (EIS) and Microwave Impedance Spectroscopy (MIS) probes, and finally (iii) by direct measurement in *ex vivo* breast cancer specimens with both EIS and MIS probes. The significance of this study is that it involved *in vivo* measurements. The results of this study are summarised in Figure 5.

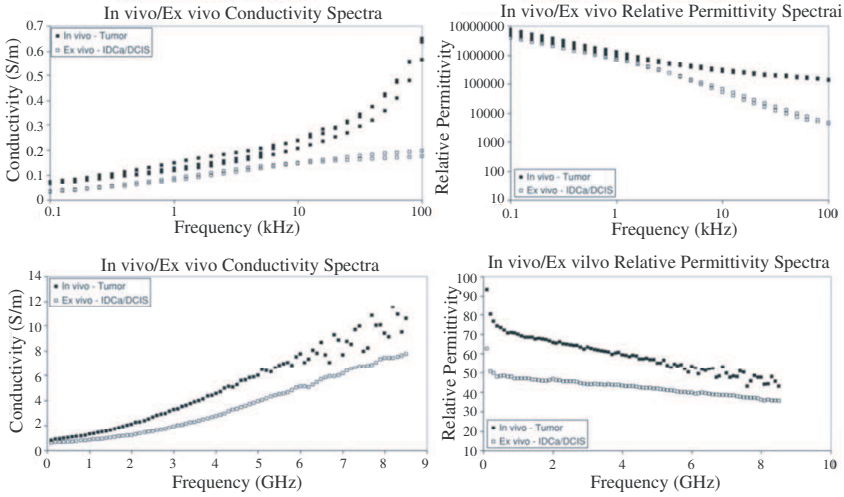

Figure 5. In vivo versus ex vivo dielectric spectra (EIS top and MIS bottom). Multiple spectra recorded for EIS are shown, while the average MIS spectrum is illustrated. Images are reproduced from [41].

In [41], it was observed that the dielectric properties for normal breast tissue estimated in scenario (i) agreed with the findings from previous studies, such as Lazebnik's [15]. Furthermore, the estimations of dielectric properties in scenario (iii) also agreed well with previous *ex vivo* studies such as [37, 38, 40, 42]. However, Haemmerich et al. [43] observed a change in some dielectric parameters after excising tissue and attributed those changes to variations of temperature, tissue dehydration and ischemic effects. Moreover, they also noted that those changes may occur within seconds after extraction of tissues and may stabilize for hours thereafter. Finally, for scenario (ii) in Halter's study, it was found that values for conductivity and relative permittivity of breast cancer were significantly higher than those estimated in scenarios (i) or (iii).

4.2. Tumour Modelling

To aid in the development of classification algorithms, it is often necessary to develop a database of tumour models which incorporates different tumour sizes and growth patterns. Two methods have principally been used for tumour modelling in 2D and in 3D studies: polygonal approximation using an elliptical baseline [44–49] and Gaussian Random Spheres [30, 35, 50–57]. The basis for these methods

is described in the following subsections.

4.2.1. Polygonal Approximation Using an Elliptical Baseline Method

In [45], Chen et al. presented a preliminary study addressing the effect of the morphology of a tumour mass on microwave signature in 2D UWB radar imaging. In their study, a 2D breast phantom was modelled with homogeneous normal breast tissue and surrounded by a layer of skin matching the Debye parameters used in [58], and tumour shapes were created based on the polygonal approximation of tumour boundaries in X-Ray mammograms by Rangayyan et al. [31]. In this method, tumours were modelled with an ellipse baseline which is then modified with two parameters, Q and ΔB, which determine the level of "ruggedness" to create tumour models — Q is the number of sides of the polygonal approximation to the tumour boundary and ΔB is the border deviation for each of the considered sides, as will be detailed and illustrated in the following text.

In studies by Chen et al. [44–48] and Teo et al. [49], a breast tumour was modelled as an infinite-length dielectric cylinder with a spiculated cross section. As these were 2D simulations, only the cylinder cross Section is considered for tumour modelling. To emulate benign and malignant tumours, the first stage is to establish the elliptical behaviour of the masses. $B(\varphi)$ represents the boundary of the ellipse baseline which is defined in the polar coordinate as:

$$B(\varphi) = \frac{ab}{\sqrt{a^2 \sin^2 \varphi + b^2 \cos^2 \varphi}} \tag{1}$$

where a and b are the lengths of the semi-major and semi-minor axes of the baseline ellipse, and φ is the angle from the positive x-axis, as indicated in Figure 6(a).

The initial elliptical shape of tumours is then modified to produce the different mass borders as follows:

- Firstly, the number of sides of the polygonal approximation to the tumour boundary, Q, is defined.
- Secondly, a distribution function of φ is set. In brief, it is assumed that the baseline ellipse is approximated by a Q-sided polygon, where $\varphi_q \in U[0, 2\pi]$, $(q \in 1, 2, \ldots, Q)$ denoted the angle of each vertex of the Q-sided polygon with respect to the x-axes, U denotes a uniform distribution.
- For each φ_q, the border deviation profile is defined: $\zeta(\varphi_q) \in U(-\Delta B, +\Delta B)$. Consequently, the final border of the tumour is given by $B'(\varphi) = B(\varphi)(1 + \zeta(\varphi_q))$.

In order to vary the level of ruggedness of the different tumour boundaries, parameters Q and ΔB are varied. As $Q \rightarrow +\infty$ and $\Delta B \rightarrow 0$, the tumour border approaches to a perfect ellipse. In Figures 6(b)–(d), the border of three different tumours with three different sets of Q and ΔB are shown. The boundaries of different regions are defined by different sets of polygons that radiate out from the centre of the tumour.

4.2.2. Gaussian Random Sphere Method

The mathematical model for Gaussian Random Spheres (GRSs) was developed and presented by Muinonen [59–61], and later adjusted to the breast tumour context by Davis et al. [30]. The shape of the GRS is given by a radius vector, $\mathbf{r} = \mathbf{r}(\boldsymbol{\vartheta}, \boldsymbol{\varphi})$, which is defined by the logradius (logarithmic radius), $\mathbf{s} = \mathbf{s}(\boldsymbol{\vartheta}, \boldsymbol{\varphi})$:

$$r(\vartheta, \varphi) = \alpha \exp\left[\mathbf{s}(\vartheta, \varphi) - \frac{1}{2}\beta^2\right] \tag{2}$$

$$s(\vartheta, \varphi) = \sum_{l=0}^{\infty} \sum_{m=-l}^{l} s_{lm} Y_{lm}(\vartheta, \varphi) \tag{3}$$

In the equations above (ϑ, φ) stand for the spherical coordinates, α is the mean radius, β is the standard deviation of the logradius, Y_{lm} are the orthonormal spherical harmonics, s_{lm} are the spherical harmonics weight coefficients, and l and m stand for the degree and order of the expansion.

Furthermore, the covariance functions of the radius and the logradius, $\alpha^2 \Sigma_{\mathrm{r}}$ and Σ_s, respectively, and the corresponding variances,

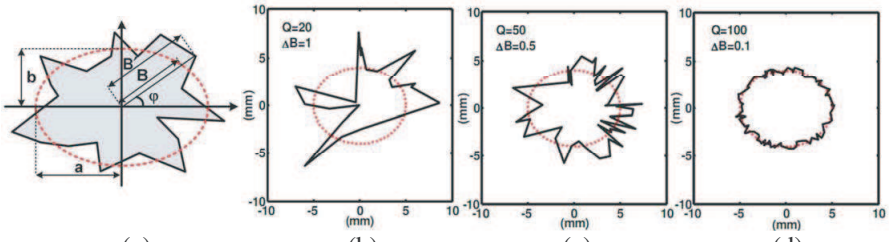

Figure 6. (a) Schematic drawing of a 2D breast phantom. (b)–(d) Examples of border deviation profiles which depend on the variation of parameters Q and ΔB [45].

$\alpha^2\sigma^2$ and β^2, are interrelated through:

$$\Sigma_r = \exp(\Sigma_s) - 1 \tag{4}$$

$$\sigma^2 = \exp(\beta^2) - 1 \tag{5}$$

in which σ represents the standard deviation of the radius. The covariance function of the logradius can be further given by:

$$\Sigma_s = \beta^2 C_s(\gamma) \tag{6}$$

in which, γ is the angular distance between two directions (ϑ_1, φ_1) and (ϑ_2, φ_2), and C_s is the logradius correlation function. After adjusting for the degree of the expansion (l) as in [60], the correlation length ℓ and the correlation angle Γ are defined by:

$$\ell = \frac{1}{\sqrt{-C_s^{(2)}(0)}} \tag{7}$$

$$\Gamma = 2\arcsin\left(\frac{1}{2}\ell\right) \tag{8}$$

in which $C_s^{(2)}$ is the logradius correlation function for which $\Sigma_s^{(2)}$ is the second derivative of the covariance function with respect to $\gamma = 0$ (Equation (6)). GRSs can be modified mathematically to model both malignant and benign tumours of different sizes by varying the mean radius (α) and the covariance function of the logradius (Σ_s) [60]. It is commonly accepted that malignant tumours take microlobulated and spiculated shapes, whereas benign tumours take smooth and macrolobulated shapes.

Microlobulated, macrolobulated and smooth GRSs are obtained by varying the correlation angle (Γ): studies have varied this angle in intervals of 5°. The correlation angle varies between 5° and 20° approximately for microlobulated GRSs, between 25°and 45° for macrolobulated GRSs and between 50° and 90° for smooth GRSs. Microlobulated GRSs are often represented by spherical volumes with several smaller lobular protuberances of different sizes on the surface. Macrolobulated GRSs often resemble ellipsoid figures in which one of the dimensions is significantly higher than the other or show large lobular protuberances. Smooth GRSs have a spherical or ellipsoid appearance with light distortions on the surface.

Spiculated GRSs are obtained by adding 3, 5 or 10 spicules to smooth GRSs, as firstly used in [30]. The increasing number of spicules reflects the evolution of the tumour model as it suggests that the tumour is spreading in more directions. The spicules are modelled with cones of height 2 cm and with a radius matching the average radius of the smooth GRSs to which they are added. Consequently, this implies

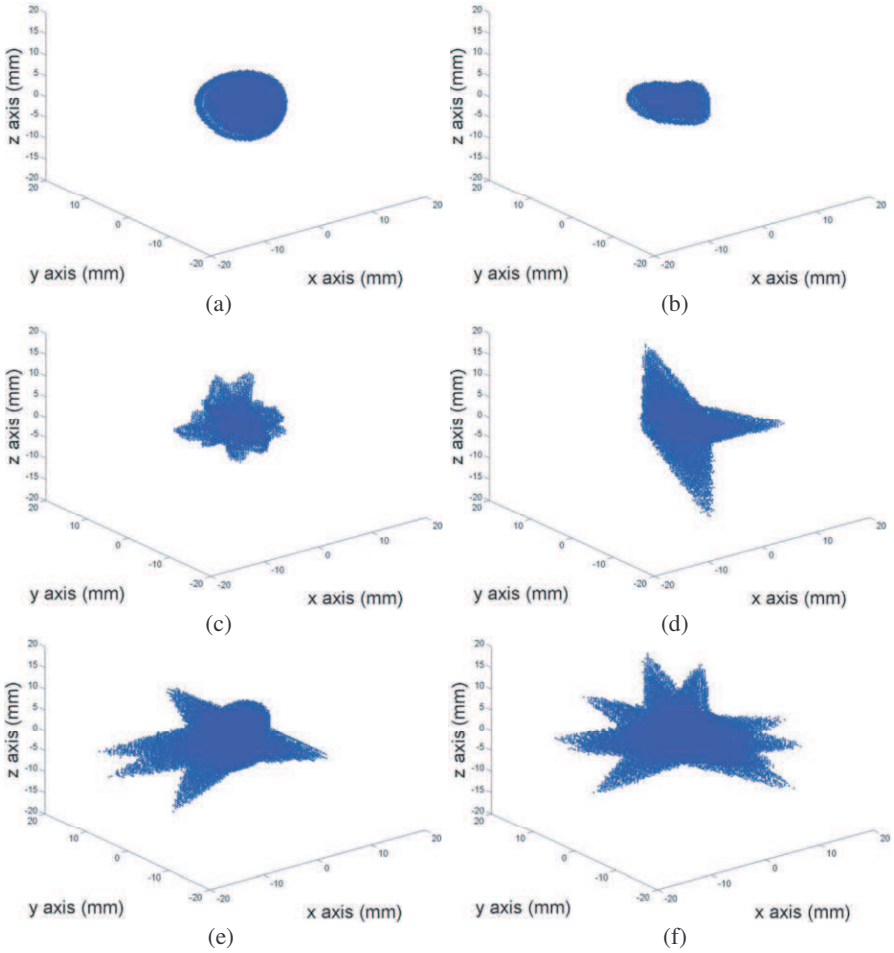

Figure 7. Samples for different Gaussian Random Spheres (GRSs) representing benign and malignant tumour models: (a) smooth, (b) macrolobulated, (c) microlobulated, (d) spiculated with 3 spicules, (e) spiculated with 5 spicules, and (f) spiculated with 10 spicules. The GRS models have an average radius size of 5 mm.

that the spicules are more prominent for GRSs with smaller average radii than for GRSs with larger average radii, as the length of the spicules remains constant. Finally, the centre of the GRSs matches the centre of the base of the spicules which are randomly assigned to a random direction. Examples of benign and malignant tumour models based on the GRSs method, with radii of 5 mm, are shown in Figure 7.

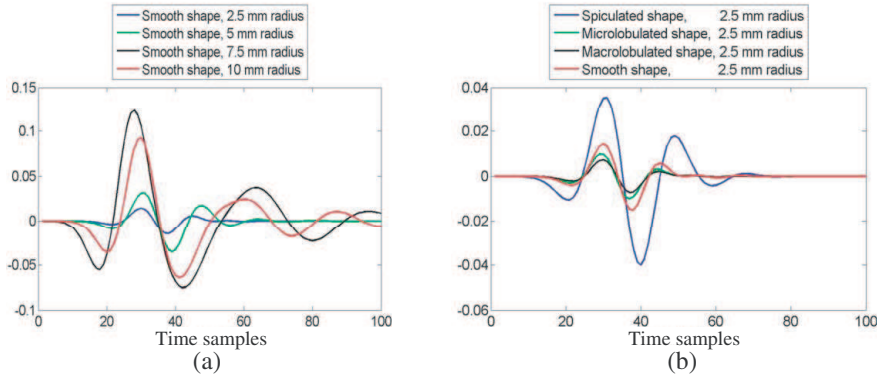

Figure 8. Sample of (a) backscattered signals for tumours of identical shape with different sizes and (b) backscattered signals for tumours of different shapes with identical size.

Numerical simulations, such as those later described in subsection 4.4 allow for the acquisition of the backscattered response of tumours embedded in breast models. As an example, the backscattered signals of a smooth tumour with different values of radii, and the backscattered signals of the smallest tumours (with a radius of 2.5 mm) with different shapes are presented in Figure 8 to illustrate the differences between the signals produced by tumours of different sizes and shapes, hereby presented. These illustrative results correspond to a very simple homogeneous breast model, but are indicative that tumour classification based on its Radar Target Signature is possible.

It must be noted that the smooth tumours are not geometrically the same for all sizes, which explains why, for Figure 8(a) there is not a linear correlation between the amplitude of the backscattered signals and the radii of tumour models.

4.3. Breast Tissue Modelling

Apart from tumour modelling, an accurate numerical model of the remainder of the breast is required to examine the performance of microwave imaging and classification algorithms. A database of such models has been made available in the University of Wisconsin Computational Electromagnetics Laboratory (UWCEM) Numerical Breast Phantom Repository [62, 63]. These MRI-derived Finite Difference Time Domain (FDTD) model preserve the anatomical

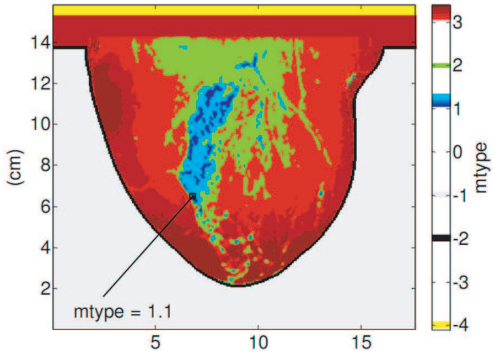

Figure 9. Example of the spatial distribution of tissue types within the models provided by the UWCEM repository (sagittal slice from a 3D numerical breast phantom, breast ID: 012204 [63]).

structure and tissue distribution within the breast. The phantoms were created by transforming 3D MRIs of the breast. For each breast MRI, each voxel was mapped to appropriate dielectric properties in the corresponding FDTD phantom.

In the UWCEM Numerical Breast Phantom Repository, a database of 9 breast models has been created. Breast models are categorised in terms of the ratio between fibroglandular and adipose tissue: "mostly fat" (2 models), "scattered fibroglandular" (3 models), "heterogeneously dense" (3 models), "very dense" (1 model). The dispersive properties of breast tissue can be incorporated into the FDTD model using a single-pole Debye model. The FDTD Grid resolution is specified as $(1\,\text{mm} \times 1\,\text{mm} \times 1\,\text{mm})$ and the time step dt is defined as 0.833 ps ($dt = dx/c_0$). The FDTD Grid can be terminated on each side by a Uniaxial Perfectly Mached Layer (UPML) in order to minimize edge reflections. An example of a breast phantom from the UWCEM Numerical Breast Phantom Repository is shown in Figure 9.

4.4. Combining Breast and Tumour Models

UWB tumour classification was examined by Chen et al. [44–48] and Teo et al. [49] using tumours located in 2D breast models, while studies by Davis et al. [30] and Conceição [51–55], McGinley et al. [56], O'Halloran et al. [57] and Alshehri et al. [64] considered tumours in 3D breast models. The latter will not be further discussed in this study since discrimination between benign and malignant tumours is only assessed in terms of dielectric differences between the two types of tumours and does not address resulting tumour signatures due to

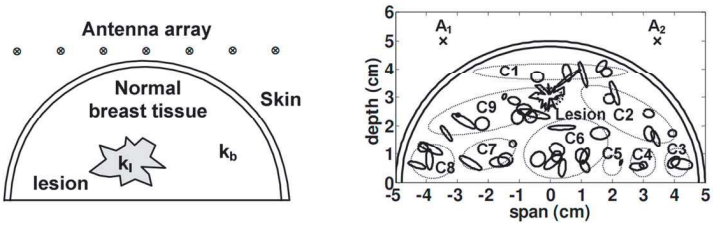

Figure 10. Set-ups of the 2D FDTD lattice with the indication of the antennas in the studies by Chen et al. [45] (a) and Chen et al. [44, 47, 48] (b).

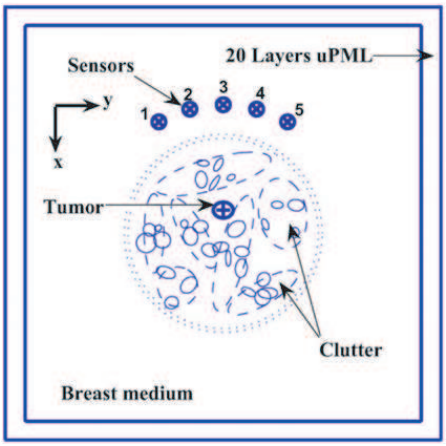

Figure 11. 2D FDTD Breast model as used by Teo et al. [49].

different shapes, which is the scope of this paper.

Chen et al. created two different breast models to use with a planar array of antennas: a simple model that comprises normal breast tissue, skin and the tumour tissue [45], represented in Figure 10(a); and a more complex breast model comprising normal breast tissue with several regions of fibroglandular clusters around the tumour, the tumour itself and skin tissue [44, 47, 48], shown in Figure 10(b).

Teo et al. [49] created a breast model for use with a circular array of antennas. The breast model was similar to that in [44, 47, 48] in which regions of fibroglandular clusters surround the tumour. It should be noted that skin tissue is not included in this particular study. Figure 11 shows a representation of this model.

In Davis et al. [30], the first 3D study considering breast

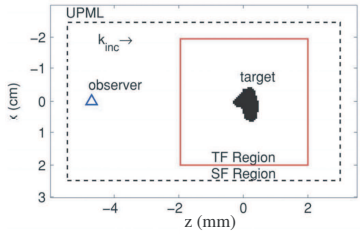

Figure 12. Cross-section of the 3D FDTD space lattice partitioned into TF and SF regions, as in the study by Davis et al. [30]. The target is illuminated by a pulsed plane wave propagating in the $+z$ direction and backscatter is recorded at the labelled observer location.

tumour classification was completed using a Total-Field/Scattered-Field (TF/SF) approach. A simple breast model was used in which only fatty breast tissue is considered with the tumour fully embedded in the TF region. The position of the antenna is indicated by the observer position, as illustrated in Figure 12.

In studies by Conceição et al. [51–53, 55] and McGinley et al. [56] a similar approach to that of Davis et al. [30] is used. The main differences are the dimensions of the TF and SF regions, as illustrated in Figure 13.

In the latest studies by Conceição et al. [52, 54] and O'Halloran et al. [57], dielectric heterogeneity is introduced by inclusion of fibroglandular clusters in the TF, around the tumour models. Four different breast model scenarios were considered. There were two Models (I and II) in which a cluster of fibroglandular tissue is positioned at a fixed location within the breast and two different Models (III and IV) in which there are one and two moving cluster (s) of fibroglandular tissue. For Model I, the portion of heterogeneous breast tissue is located within the cubic TF region in one of its vertices. For Model II, the same block of heterogeneous breast tissue is also located within the TF region, at a different distance from one vertex of the cubic TF region. For Model III the cluster of heterogeneous breast tissue is randomly located within the TF region. For Model IV two independent clusters of heterogeneous breast tissue are randomly located in a pair of locations. The TF of Models I, II, III and IV are illustrated in Figure 14.

The main significant difference between this study and previous studies is the fact that the location of the fibroglandular tissue is randomly varied between simulations (Models III and IV). If the fibroglandular tissue location is fixed (such as in Models I and II) and in models of studies by Chen et al. [44, 48] and Teo et al. [49],

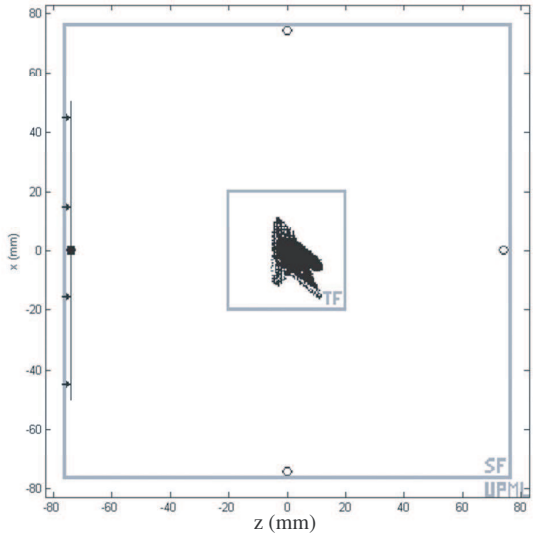

Figure 13. Cross-section of the 3D FDTD space lattice partitioned into TF, SF and UPML regions, for a homogeneous breast model. The target is located at the centre of the TF and is illuminated by a pulsed plane wave (represented by a dark line) and backscatter is recorded at the first antenna (represented by a filled circle). Antennas are represented by small circles.

the classifier can be trained to "ignore" its response, making tumour classification much simpler than what it actually is. A much more realistic scenario is to have the position of the fibroglandular tissue varied between simulations, making it impossible for the classifier to "ignore" the noise due to dielectric heterogeneity.

5. CONCLUSION

This paper provides a basis for the development of more geometrically and dielectrically accurate numerical breast phantoms with embedded tumours used in the development of robust microwave imaging and classification algorithms. The paper examines the anatomy and physiology of the breast and the growth and development of breast cancer. From a modelling perspective, the paper discusses the various studies examining the dielectric properties of normal and cancerous breast tissue, while also considering various methods to representatively model the breast, and benign and malignant tumours.

Section 2 presented the anatomy and physiology of the breast,

and the interconnection between different types of tissue is considered. Section 3 examined the most frequently-occurring types of breast tumours, how they are formed in a cellular context, and also how these changes affect dielectric properties.

In Section 4, studies examining the dielectric properties of the breast were reviewed, focusing in particular on recent studies by Lazebnik and Halter. Tumour modelling methods were reviewed: 2D models based on polygonal approximation using an elliptical baseline method and 3D models based on Gaussian Random Spheres. Modelling techniques are also reviewed, describing how MRI data is mapped to FDTD breast phantoms. Finally, an FDTD model incorporating realistic tumour models is presented, and the subject of breast heterogeneity is given particular attention.

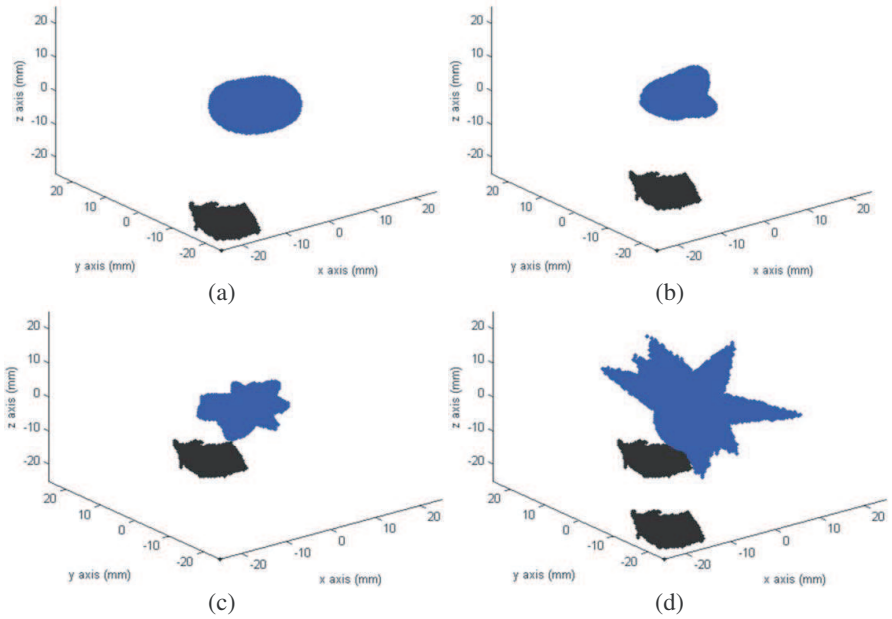

Figure 14. TF of different breast models [52, 54, 57] in which tumours are represented in blue and fibroglandular clusters are represented in black. The (a) smooth and (b) macrolobulated tumour models are represented in Models I and II, respectively. The (c) microlobulated and (d) spiculated (10 spicules) tumour models are represented in random samples of Models III and IV, respectively.

REFERENCES

1. American Cancer Society, *Cancer Facts & Figures*, Atlanta, 2008.
2. Nass, S. L., et al., *Mammography and Beyond: Developing Technologies for the Early Detection of Breast Cancer*, National Academy Press, 2001.
3. Lehman, C. D., et al., "MRI evaluation of the contralateral breast in women with recently diagnosed breast cancer," *The New England Journal of Medicine*, Vol. 356, No. 13, 1295–1303, 2007.
4. Viehweg, P., et al., "Contrast-enhanced magnetic resonance imaging of the breast: interpretation guidelines," *Top Magn Reson Imaging*, Vol. 9, No. 1, 17–43, 1998.
5. Maestro, C., et al., "Systematic ultrasonography in asymptomatic dense breasts," *Eur. J. Radiol.*, Vol. 26, No. 3, 254–256, 1998.
6. Wang, L., et al., "Microwave-induced acoustic imaging of biological tissues," *Rev. Sci. Instrum*, Vol. 70, No. 9, 3744–3748, 1991.
7. Souvorov, A. E., et al., "Two-dimensional computer analysis of a microwave flat antenna array for breast cancer tomography," *IEEE Trans. on Microwave Theory and Tech.*, Vol. 48, No. 8, 1413–1415, 2000.
8. Bulyshev, A. E., et al., "Computational modeling of three-dimensional microwave tomography of breast cancer," *IEEE Trans. on Biomed. Eng.*, Vol. 48, No. 9, 1053–1056, 2001.
9. Meaney, P. M., et al., "A clinical prototype for active microwave imaging of the breast," *IEEE Trans. on Microwave Theory and Tech.*, Vol. 48, No. 11, 1841–1853, 2000.
10. Meaney, P. M., et al., "Nonactive antenna compensation for fixed-array microwave imaging: Part II—Imaging results," *IEEE Trans. on Med. Imag.*, Vol. 18, No. 6, 508–518, 1999.
11. Liu, Q. H., et al., "Active microwave imaging I — 2-D forward and inverse scattering methods," *IEEE Trans. on Microwave Theory and Tech.*, Vol. 50, No. 1, 123–133, 2002.
12. Hagness, S. C., et al., "Two dimensional FDTD analysis of a pulsed microwave confocal system for breast cancer detection: Fixed-focus and antenna-array sensors," *IEEE Trans. on Biomed. Eng.*, Vol. 45, 1470–1479, 1998.
13. Bindu, G., et al., "Active microwave imaging for breast cancer detection," *Progress In Electromagnetics Research*, Vol. 58, 149–169, 2006.
14. Sha, L., et al., "A review of dielectric properties of normal

and malignant breast tissue," *IEEE SoutheastCon*, 457–462, Columbia, SC, USA, 2002.

15. Lazebnik, M., et al., "A large-scale study of the ultrawideband microwave dielectric properties of normal breast tissue obtained from reduction surgeries," *Phys. Med. Biol.*, Vol. 52, 2637–2656, 2007.
16. Bland, K. I., et al., *The Breast: Comprehensive Management of Benign and Malignant Disorders*, Elsevier, Vol. 1, 2004.
17. Jossinet, J., "The impedivity of freshly excised human breast tissue, *Physiol. Meas.*, Vol. 19, No. 1, 61–75, 1998.
18. Hagness, S. C., et al., "Three-dimensional FDTD analysis of a pulsed microwave confocal system for breast cancer detection: design of an antenna-array element," *IEEE Trans. on Antennas and Propagat.*, Vol. 47, No. 5, 783–791, 1999.
19. Choi, J. W., et al., "Microwave detection of metastasized breast cancer cells in the lymph node; potential application for sentinel lymphadenectomy," *Breast Cancer Res. and Treat.*, Vol. 86, 107–115, 2004.
20. Gorey, T., et al., *The Breast in Health and Illness — An Information Guide for Patients and Their Carers (DVD)*, AstraZeneca Pharmaceuticals (Irl.) Ltd. Dublin, Ireland, 2006.
21. CancerHelp UK, *Breast Cancer Section Overview*, 2007, http://www.cancerhelp.org.uk/help/default.asp?page=3270.
22. Enzinger, F. M., et al., *Soft Tissue Tumors*, 3rd edition, Mosby, Year Book, Inc., Missouri, 1995.
23. Dixon, J. M., *ABC of Breast Diseases*, 3rd edition, Blackwell Publishing Ltd., 2006.
24. CancerHelp UK, *About Cancer*, 2007, http://www.cancerhelp.org.uk/help/default.asp?page=85.
25. Cameron, I. L., et al., *The Transformed Cell*, Cell Biology, A Series of Monographs, Academic Press, New York, 1981.
26. Bridges, J. E., et al., *Microwave Discrimination between Malignant and Benign Breast Tumours*, Patent No.: US 6,431,550 B1, Assignee: L.L.C. Interstitial, USA, 2002.
27. Malich, A., et al., "The impact of lesion vascularisation on tumours detection by electrical impedance scanning at 200 Hz," *Biomed Imaging Interv J.*, 3(4:e33), 2007.
28. Joines, W. T., "Frequency-dependent absorption of electromagnetic energy in biological tissue," *IEEE Trans. on Biomed. Eng.*, Vol. 31, No. 1, 17–20, 1984.
29. Pethig, R., "Dielectric properties of biological materials:

Biophysical and medical applications," *IEEE Trans. on Electr. Insul.*, Vol. E1–19, No. 5, 453–474, 1984.

30. Davis, S. K., et al., "Breast tumor characterization based on ultrawideband microwave backscatter," *IEEE Trans. on Biomed. Eng.*, Vol. 55, No. 1, 237–246, 2008.
31. Rangayyan, R. M., et al., "Measures of acutance and shape for classification of breast tumors," *IEEE Trans. on Med. Imag.*, Vol. 16, No. 6, 799–810, 1997.
32. Bindu, G., et al., "Characterization of benign and malignant breast tissues using 2-D microwave tomographic imaging," *Microw. Opt. Technol. Lett.*, Vol. 49, 2341–2345, 2007.
33. Nguyen, T. M., et al., "Shape analysis of breast masses in mammograms via the fractial dimension," *Engineering in Medicine and Biology 27th Annual Conference*, 3210–3213, Shangai, China, 2005.
34. Guliato, D., et al., "Polygonal modeling of contours of breast tumors with the preservation of spicules," *IEEE Trans. on Biomed. Eng.*, Vol. 55, No. 1, 14–20, 2008.
35. O'Halloran, M., et al., "FDTD modeling of the breast: A review," *Progress In Electromagnetics Research B*, Vol. 18, 1–24, 2009.
36. Joines, W. T., et al., "The measured electrical properties of normal and malignant human tissues from 50 to 900 MHz," *Med. Phys.*, Vol. 21, No. 4, 1994.
37. Lazebnik, M., et al., "A large-scale study of the ultrawideband microwave dielectric properties of normal, benign and malignant breast tissues obtained from cancer surgeries," *Phys. Med. Biol.*, Vol. 52, 6093–6115, 2007.
38. Campbell, A. M., et al., "dielectric properties of female human breast tissue measured *in vitro* at 3.2 GHz," *Phys. Med. Biol.*, Vol. 37, No. 1, 193–210, 1992.
39. Chaudhary, S. S., et al., "Dielectric properties of normal and malignant human breast tissues at radiowave and microwave frequencies," *Indian J. Biochem. Biophys.*, Vol. 21, 76–79, 1984.
40. Surowiec, A. J., et al., "Dielectric properties of breast carcinoma and the surrounding tissues," *IEEE Trans. on Biomed. Eng.*, Vol. 35, No. 4, 257–263, 1988.
41. Halter, R. J., et al., "The correlation of *in vivo* and *ex vivo* tissue dielectric properties to validate electromagnetic breast imaging: Initial clinical experience," *Physiol. Meas.*, Vol. 30, No. 6, S121–S136, 2009.
42. Jossinet, J., et al., "A review of parameters for the bioelectrical

characterization of breast tissue," *Ann. N.Y. Acad. Sci.*, Vol. 873, 30–41, 1999.

43. Haemmerich, D., et al., "Changes in electrical resistivity of swine liver after occlusion and postmortem," *Med. Biol. Eng. Comput.*, Vol. 40, No. 1, 29–33, 2002.
44. Chen, Y., et al., "Application of the mimo radar technique for lesion classification in UWB breast cancer detection," *17th EUSIPCO*, 759–763, Glasgow, Scotland, 2009.
45. Chen, Y., et al., "Effect of lesion morphology on microwave signature in ultra-wideband breast imaging: A preliminary two-dimensional investigation," *IEEE Antennas and Propagation Society International Symposium*, 2168–2171, 2007.
46. Chen, Y., et al., "Effect of lesion morphology on microwave signature in 2-D ultra-wideband breast imaging," *IEEE Trans. on Biomed. Eng.*, Vol. 55, No. 8, 2011–2021, 2008.
47. Chen, Y., et al., "Multiple-input multiple-output radar for lesion classification in ultrawideband breast imaging," *IEEE Journal of Selected Topics in Signal Processing*, Vol. 4, No. 1, 187–201, 2010.
48. Chen, Y., et al., "Feasibility study of lesion classification via contrast-agent-aided uwb breast imaging," *IEEE Trans. on Biomed. Eng.*, Vol. 57, No. 5, 1003–1007, 2010.
49. Teo, J., et al., "Breast lesion classification using ultrawideband early time breast lesion response," *IEEE Trans. on Antennas and Propagat.*, Vol. 58, No. 8, 2604–2613, 2010.
50. Conceição, R. C., et al., "Antenna configurations for ultra wide band radar detection of breast cancer," *SPIE BIOS West*, Vol. 7169, No. 9, [71691M, 12], San José, CA, USA, 2009.
51. Conceição, R. C., et al., "Support vector machines for the classification of early-stage breast cancer based on radar target signatures," *Progress In Electromagnetics Research B*, Vol. 23, 311–327, 2010.
52. Conceição, R. C., et al., "Evaluation of features and classifiers for classification of early-stage breast cancer," *Journal of Electromagnetic Waves and Applications*, Vol. 25, No. 1, 1–14, 2011.
53. Conceição, R. C., M. O'Halloran, D. Byrne, E. Jones, and M. Glavin, "Tumor classification using radar target signatures," *PIERS Proceedings*, 346–349, Cambridge, MA, USA, July 5–8, 2010.
54. Conceição, R. C., et al., "Effects of dielectric heterogeneity in the performance of breast tumour classifiers," *Progress In*

Electromagnetics Research M, Vol. 17, 73–86, 2011.

55. Conceição, R. C., et al., "Investigation of classifiers for early-stage breast cancer based on radar target signatures," *Progress In Electromagnetics Research*, Vol. 105, 295–311, 2010.
56. McGinley, B., et al., "Spiking neural networks for breast cancer classification using radar target signatures," *Progress In Electromagnetics Research C*, Vol. 17, 79–94, 2010.
57. O'Halloran, M., et al., "Spiking neural networks for breast cancer classification in a dielectrically heterogeneous breast," *Progress In Electromagnetics Research*, Vol. 113, 413–428, 2011.
58. Bond, E. J., et al., "Microwave imaging via space-time beamforming for early detection of breast cancer," *IEEE Trans. on Antennas and Propagat.*, Vol. 51, No. 8, 1690–1705, 2003.
59. Muinonen, K., "Introducing the gaussian shape hypothesis for asteroids and comets," *Astron. and Astrophys.*, Vol. 332, 1087–1098, 1998.
60. Muinonen, K., "Chapter 11: Light scattering by stochastically shaped particles," *Light Scattering by Nonspherical Particles: Theory, Measurements, and Applications*, M. I. Mishchenko, J. W. Hovenier, and L. D. Travis (eds.), Academic Press, 2000.
61. Muinonen, K., *Gaussian Random Sphere Program G-sphere*, 2002, Last accessed: 23/05/2008; Available from: www.astro.helsinki.fi/psr/
62. *University of Wisconsin — Computational Electromagnetics Laboratory (UWCEM)*, http://uwcem.ece.wisc.edu/.
63. Zastrow, E., et al., *Database of 3D Grid-Based Numerical Breast Phantoms for Use in Computational Electromagnetics Simulations*, http://uwcem.ece.wisc.edu/home.htm.
64. Alshehri, S. A., et al., "3D experimental detection and discrimination of malignant and benign breast tumor using NN-based UWB imaging system," *Progress In Electromagnetics Research*, Vol. 116, 221–237, 2011.